



## A Data Model for In-stream Forces on a Cylinder Using Neural Networks and Linear Prediction Filters

Erdem Aktosun<sup>1,2</sup>, Nikolaos I Xiros<sup>1\*</sup> and Jason M Dahl<sup>2</sup>

<sup>1</sup>Naval Architecture and Marine Eng., University of New Orleans, USA

<sup>2</sup>Ocean Engineering, University of Rhode Island, USA

\*Corresponding Author: Nikolaos I Xiros, Naval Architecture and Marine Eng., University of New Orleans, USA.

Received: May 20, 2021

Published: July 29, 2021

© All rights are reserved by Nikolaos I Xiros, et al.

### Abstract

Hydrodynamic force and error estimation model are developed based on experimental data. Force model is developed to model the dynamic forces with Artificial Neural Network (ANN) on an oscillating circular cylinder for flow conditions where Vortex-Induced-Vibrations (VIV) are known to occur and data error estimation model is developed for this existing neural network time dependent hydrodynamic force model. The force and error estimation model are developed to use in potential control systems to improve VIV based energy harvesting. The dynamic model is empirical, utilizing force measurements obtained for a large set of forced motion experiments, spanning a range of parametric values that prescribe the kinematics of the cylinder motion. The model includes the dynamics of a circular cylinder undergoing forced combined in-line and cross-flow motion in a free stream. The experiments were conducted in a fully automated towing tank where parameters of in-line amplitude of motion, cross-flow amplitude of motion, reduced velocity, and phase difference between in-line and cross-flow motion were varied over nearly 10,000 experiments. All experiments were carried out at a constant Reynolds number of 7620. A feed forward neural network is trained using the force database to develop a time dependent model of forces on the cylinder for given kinematic conditions. The time series error between the measured and feed forward Artificial Neural Network (ANN) model is found for the lift and drag force time histories. An autoregressive (AR) error predictor is developed from the existing neural network time dependent model of forces on the cylinder for given kinematic conditions. This error predictor is developed based on the error between the measured signal and artificial neural network model and can be used to improve predictions from the model.

**Keywords:** Vortex Induced Vibrations; Neural Networks; Data Analysis; Autoregressive Filter; Linear Prediction

### Introduction

Fluid-structure interactions (FSIs), such as vortex-induced vibrations (VIV), are widespread and fundamental engineering problems in the general fields of hydrodynamics and dynamical systems. The phenomenon of vortex-induced vibrations is typically observed in long slender structures that encounter fluid flows in their operating environment, such as deep sea drilling risers, oil platforms, cooling towers and wind turbines, etc. This phenomenon causes vibration of the structure as vortices shedding in the wake of the structure excites the natural frequency of the struc-

ture and in turn the fluid shedding phenomenon couples with the excited motion of the structure. These vibrations can lead to fatigue problems and limit the operation of offshore, due to increased loading on the structure when vibrating. The fundamental problem of VIV has been extensively studied by researchers due to its prevalence in many engineering applications [1-6]. More recently, the phenomenon has been proposed as a potential technique for energy harvesting [7]. In energy harvesting applications, focus has primarily been on the vibration of elastically mounted circular cylinders in a current that are constrained to cross-flow motion or motion perpendicular to the direction of the current. In order to

improve power output in energy harvesting, allowing the cylinder to move with combined in-line and cross-flow motion relative to the direction of the fluid has the ability to increase the amplitude response of the system, increasing power output. Therefore, developing dynamical models that can predict the forcing and behavior a this type of system is necessary for developing control strategies for VIV-based energy harvesters.

Previous work has demonstrated that combined in-line and cross-flow motion enhances both the cross-flow amplitude response of a circular cylinder undergoing VIV and results in higher harmonic forcing in the lift direction. In traditional engineered systems, this can lead to increased fatigue in structures subject to this fluid-structure interaction [8,9] due to the very large amplitude motions [10], but in energy harvesting systems, these larger amplitude motions could be controlled to increase energy harvesting capability. Since the coupling between motion and fluid forces is linked non-linearly through the time dependent shedding of vortices, it is difficult to develop simple fluid force models that can predict the fluid-structure coupling. Semi-empirical methods have improved efforts for modeling fluid forces by utilizing empirically derived data from free vibration or forced motion experiments to estimate fluid forces when coupled with a structural model.

Semi-empirical prediction methods that employ simple structural models combined with an empirical database derived from forced motion experiments, such as those in [11-14], have been shown to be better predictors of cross-flow motion VIV due to the direct use of real measured forces in the coupling prediction [15]. However, extension of these semi-empirical methods to include combined cross-flow and in-line motion are often unwieldy due to the sheer number of experiments necessary in order to provide a well resolved database of force measurements since including in-line motion significantly increases the number of variables describing the body motion. This semi-empirical approach has been developed for improving predictive capabilities in energy harvesting applications [16], but has not yet been extended to systems with combined in-line and cross-flow motion in energy harvesting. In addition, time-varying hydrodynamic coefficient models have been studied to predict VIV [17,18] for these types of applications as well. While previous forced motion experiments studying the combined in-line and cross-flow motion have been performed over a sparse parameter space including variations of cross-flow amplitude,

in-line amplitude, reduced velocity, and phase between in-line and cross-flow motion [19], the resulting force databases from this work have not yet been successfully implemented in predictive tools for VIV. This dataset has been extended for resolving the lower amplitude parameter space further to investigate the use of the dataset for semi-empirical prediction [20], however limited analysis of the resulting forces from combined in-line and cross-flow motions have ensued from these studies. A more resolved database has been developed [21,22] through the use of a unique automated experimental apparatus to construct a database of forced combined in-line and cross-flow motions at a particular Reynolds number, providing a rich source of hydrodynamic force data that can be used for developing artificial intelligence based predictive force models.

In the study, the force database of [21] is utilized to develop a dynamical model of the time dependent force acting on a cylinder undergoing forced combined in-line and cross-flow motion. A feed forward neural network is trained using the force measurements to develop time dependent models of forces on the cylinder for given cylinder kinematics. There is some error between the measured force on the body and the predicted time dependent force. Also, we develop an error estimation model for the existing neural network time dependent hydrodynamic force model in order to improve the neural network model. The error estimator is created from this neural network time dependent model of forces on the cylinder for given kinematic conditions by using autoregressive (AR) filtering. The autoregressive technique allows for advanced prediction of errors to help improve the time dependent prediction from the neural network model. We develop this technique because data-driven of modeling, prediction and control complex dynamical systems are very important in fluid-structure interactions. The most challenging scientific problem in that current empirical models or derivations are not responsive these kind of non-linear dynamic systems. Thus, data analysis and force modelling approaches are required to achieve in depth understanding of the physics governing this kind of complex dynamical systems. The significance and major contribution of this work is that this developed ANN force and error estimation model might be a good foundation to improve for further modeling, prediction and control system for complex dynamical systems of two-degree-of-freedom. This analysis could be utilized for further experimental analysis for two-degree-of-freedom VIV systems.

### Experimental Details

Automated forced two-degree-of-freedom experiments were conducted in the experimental fluid mechanics laboratory at the University of Rhode Island (URI). The experiment setup is shown in figure 1. The experiment setup consists of a towing tank, automated linear actuators, control box and data acquisition (DAQ) system. A main carriage is positioned on top of the water tank where it can move forward along the tank length with constant speed. Prescribed figure-eight and crescent forced motions of a text cylinder connected to the carriage are performed by linear actuators mounted on the carriage. While combined cross-flow and in-line VIV typically produces figure-eight and crescent shape motions of the cylinder in a carriage-fixed reference frame, the nonlinear interaction of the structural system with the fluid does not guarantee that the motions are sinusoidal in each direction. For simplicity and consistent with definitions from [10,23], we assume that to first order, the motion of the body in the in-line and cross-flow directions can be assumed to be sinusoidal, such that these motions are only defined by a single amplitude and single frequency. Additionally, consistent with observations from experiments, in-line motions are assumed to have twice the frequency of the cross-flow motion, allowing for a single frequency parameter to define the motion of the body. This helps to limit the number of variables to consider in defining the motion of the body, such that forced motions are defined as:

$$y = A_y \sin(\omega t) \text{ and } x = A_x \sin(2\omega t + \theta) \text{ -----(1)}$$

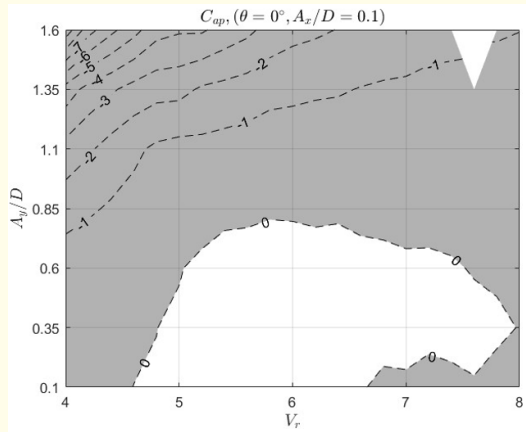


Figure 1: Pictures of the automated experimental test setup.

The phase difference between in-line and cross-flow motions,  $\theta$ , defines the orbital motion of the cylinder in the carriage fixed reference frame. The motion of the cylinder can then be defined non-dimensionally based on the non-dimensional amplitudes,  $A_y/D$  and  $A_x/D$ , a single cross-flow reduced velocity,  $V_r = (U2\pi)/(\omega D)$ , and the phase between motions,  $\theta$ . The non-dimensional parameters governing the motion of the body were varied such that the in-line amplitude is varied from 0.1 to 0.5 in increments of 0.1, the cross-flow amplitude is varied from 0.1 to 1.6 in increments of 0.25, the reduced velocity is varied from 4 to 8 in increments of 0.2 and the phase between in-line and cross-flow motions is varied from -180 degrees to 180 degrees in increments of 30 degrees. This results in a total of 9555 experiments comprising the experimental database for the single Reynolds number of 7620. Each run was performed through an automated system, such that the experiment always reset to the same starting point and waited 8.5 minutes before conducting the next experiment. Hydrodynamic forces were measured using ATI Gamma SI-65-10 and SI-130-10 six-axis force sensors.

To first order, the lift and drag forces,  $F_y$  and  $F_x$ , can be approximated as sinusoidal functions with dominant frequencies equivalent to the motion frequencies:

$$F_y = F_1 \sin(\omega t + \phi_1) \text{ and } F_x = F_2 \sin(2\omega t + \phi_2) \text{ ----- (2)}$$



**Figure 2:** Contours of the average power coefficient with variable  $Ay/D$  and  $Vr$ . Phase between motions is fixed,  $\theta = 0^\circ$  and in-line motion amplitude is fixed,  $Ax/D=0.1$ .

From the equation, the phase angles between motion and force are  $\phi_1$  and  $\phi_2$ . The portion of the force in phase with velocity of the cylinder motion will either excite or damp the motion of a freely vibrating system, dependent on the sign of the power transfer. For a system oscillating with combined in-line and cross-flow motion, this power transfer results as a function of forces in both lift and drag. We can therefore define an average power transfer coefficient,  $Cap$ , as below, where positive power transfer indicates excitation and energy transferred from the fluid to the body and negative power transfer indicates damping with energy transferred from the body to the fluid:

$$C_{ap} = \frac{\frac{1}{2} \int_0^T (F_y \cdot y + F_x \cdot x) dt}{\frac{1}{2} \rho U^3 D L} \quad (3)$$

A zero value of  $Cap$  indicates the expected response behavior of a system with zero structural damping in both in-line and cross-flow directions. Figure 2 illustrates the average power coefficient on contour plots by changing cross-flow motion amplitude and reduced velocity for fixed phase between in-line and cross-flow motion,  $\theta = 0^\circ$  and fixed in-line amplitude,  $Ax/D = 0.1$ . The expected free vibration region can be seen as the white region where  $Cap$  is positive. In previous work, the construction of the estimated force model by using neural nets were chosen from cylinder motions corresponding to this free vibration region. 26 experimental runs were chosen for building neural network and error estimators for a lift force estimator and drag force estimator based on the full measured forces.

### Force model

A discrete, time-dependent, non-linear force model is developed from the experimental data set by applying a feed forward Artificial Neural Network (ANN). The ANN is based on closed-form mathematical expressions, where weights are determined through training of the ANN [24-29]. To construct the ANN model, we define the cylinder motions (in-line and cross-flow position and velocity) as inputs to the ANN, where the force time histories in x and y are defined as outputs:

$$\hat{F}_i \equiv \hat{F}(t = nT_s) = f(a) \quad (4)$$

$$a = [x \ y \ \dot{x} \ \dot{y}]^T$$

Where  $F$  is the estimated forces from ANN and  $a$  is the input matrix of discrete positions and velocity for in-line and cross flow motions. The sampling time is defined according to the time dependent measurements from the experimental database, which is  $T_s = 0.001$  s. The function  $f$  has the following same form for lift and drag forces;

$$\hat{F} = f(a) = \vec{w}_o \cdot g(W \cdot a + \vec{b}) + b_o \quad (5)$$

Where  $W$  is the matrix including hidden weight values,  $a$  is the matrix including input values,  $b$  is column vector including hidden bias values,  $w_o$  is the row vector including output weight values,  $b_o$  is the output bias value and  $g$  is the activation function which is of the form of the tangent sigmoid function;

$$g(\xi) = \frac{e^\xi - e^{-\xi}}{e^\xi + e^{-\xi}} \quad g(\pm\infty) = \pm 1 \quad \text{and} \quad g(0) = 0 \quad (6)$$

To demonstrate the construction of the estimated force model, we select 26 experimental runs that correspond to a positive value of  $Cap$ , indicating they correspond with motions close to those observed for a self-excited vibrating system. For each experimental run condition, we define four neural network estimators, a lift force estimator based on the full measured force, a drag force estimator based on the full measured force, a lift force estimator with the fluid inertia removed, and a drag force estimator with the fluid inertia removed. The purpose for defining separate force estimators with and without the fluid inertia is that these may be used for different purposes in future control applications, where control in phase with body acceleration may be applied. The ultimate advantage of separating force estimators with and without acceleration is that the system can be trained on less data [30]. To separate the fluid inertia component from the fluid force for the neural network estimator, we train the neural network using only position and velocity values as input. When including the body acceleration, we

first express forces using a linear regression model. The linear regression is evaluated by fitting the lift and drag forces to a functional shape and the acceleration component of the model is then evaluated from the linear regression. For a linear regression force model of the form  $\hat{F} = c_1y + c_2x + c_3\dot{y} + c_4\dot{x} + c_5\ddot{y} + c_6\ddot{x}$ , we can determine the force coefficients directly through linear regression of the force measurements. Our estimated force can then be constructed by estimating the position and velocity components through the neural network model and adding the inertial components determined through linear regression, resulting in a force of the form:  $\hat{F} = FNN + c_5\dot{y} + c_6\dot{x}$ , with the linear coefficients ( $c_5$  and  $c_6$ ) calculated from the linear regression model and  $FNN$  found from neural networks based on position and velocity inputs.

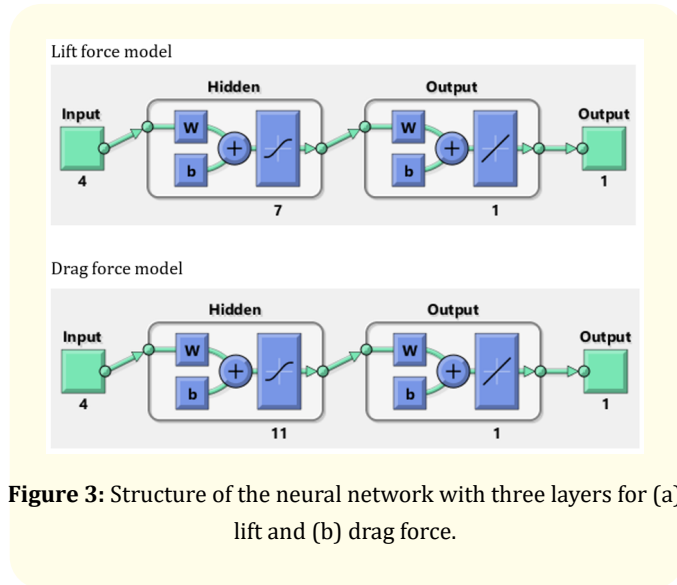


Figure 3: Structure of the neural network with three layers for (a) lift and (b) drag force.

A total of 104 neural nets (26 experiments with 4 neural networks per experiment) were derived to provide estimation of time dependent lift and drag forces with and without the portion in phase with acceleration. Figure 3 shows the structure of the neural nets for lift forces, which used 7 layers. The same neural network structure is used for drag forces, but with 11 layers. The neural nets are defined as feed forward systems, which require an input vector along with hidden and output layers. The input and output layers are linear. The input layer has 4 neurons defined as the instantaneous position in cross-flow direction, instantaneous position in in-line direction, instantaneous velocity in cross-flow direction and instantaneous velocity in in-line direction. The output layer consists of a single neuron for each neural network application. The hidden la-

yer of all cross-flow direction has 7 neurons and the hidden layer of all in-line direction has 11 neurons. All ANNs are derived through the Matlab neural network toolbox. The transfer function (activation function) of the hidden layer is the non-linear tangent sigmoid and the output layer is purely linear as mentioned earlier. Since the sampling rate of experiments was fairly high, there is good temporal resolution to the experimental data, with a large number of data points for each experimental run. To train an individual neural net for each run, 40% of the data points in the motion time history of an individual run are selected at random to be used as training data for determining weights. 40% of data points are used to train ANN model to avoid over-training. We observe good accuracy because the training data points are selected randomly. Since the system is coupled and non-linear, ANN model is essential to be used to model lift and drag time series forces. By using this ANN force model, we can develop a prediction method.

Error estimation model

Parametric modeling spectrum analysis is used to develop an error estimation model between measured forces and the deep neural network time series force model [28,31-35]. Previously, the time series of lift and drag forces were estimated from an ANN force model by using discrete position and velocity as inputsto the neural network with time dependent lift and drag force as output [36]. 26 experimental runs corresponding to free vibration region in figure 2 were used for training the ANN force model. The time series of errors between measured forces and predicted values from the ANN model are calculated for lift and drag forces as shown figure 4. The mean of the time series errors are removed,  $E = E - \langle E \rangle$ , before developing an error estimation model through an autoregressive filter. A total of 52 error signals (lift and drag force models) are investigated using a periodogram and correlogram in order to apply a power spectrum comparison. We expect the power spectrum computed using different approaches to give the same function.

The error signal in the discrete frequency domain is written as  $Ek = \sum^{N-1} Ene^{-i2\pi kn/N}$ ,  $k = 0,1,2, \dots, N - 1$ . We can compute the power spectral density of the error, function as  $S(k/NT) = |Ek|^2$  which gives the periodogram of the error signals computed directly from the Discrete Fourier Transform,  $Ek$ . A second way to compute the power spectrum of the error signals is from an analysis of the correlogram, as the power spectrum is also the Fourier transform of the autocorrelation of a signal. The autocorrelation of the error sig-

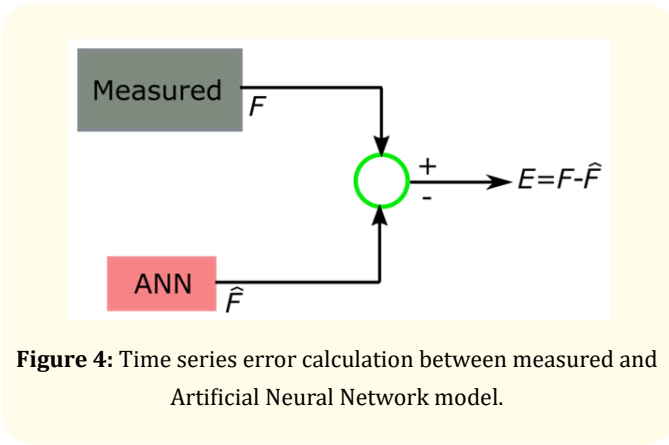


**Figure 4:** Time series error calculation between measured and Artificial Neural Network model.

nal is defined as  $R_{xx} = \sum E(r)E(r + n)$ ; where  $n$  is a time shift. By definition of the power spectral density,  $S(k/NT) = |fft(R_{xx})|$ . The periodogram and correlogram versions of the spectral density are compared to observe the structure of the signal. Also, the autocorrelation function of the time series of error can be used to categorize the error signals.

Autoregressive model is a model which depends on the previous outputs of the system. System assumes that the input signals are stationary and ergodic. The autoregressive error estimation model can be defined as:

$$E(n) = \hat{E}(n) + u(n) \tag{7}$$

$$\hat{E}(n) = \sum_{k=1}^m a_k x(n - k) \tag{8}$$

Where  $a_k, k = 1,2,3, \dots, m$ , coefficients of the autoregressive model,  $m$  is the order of the model and  $u(n)$  is the residual error of the linear autoregressive filter. In order to calculate autoregressive parameters, we need to get autocorrelation of the input signals as follows:

$$\begin{bmatrix} R_{xx}(0) & R_{xx}(1) & R_{xx}(2) & \dots & R_{xx}(m-1) \\ R_{xx}(1) & R_{xx}(0) & R_{xx}(1) & \dots & R_{xx}(m-2) \\ R_{xx}(2) & R_{xx}(1) & R_{xx}(0) & \dots & R_{xx}(m-3) \\ \dots & \dots & \dots & \dots & \dots \\ \dots & \dots & \dots & \dots & \dots \\ R_{xx}(m-1) & R_{xx}(m-2) & R_{xx}(m-3) & \dots & R_{xx}(0) \end{bmatrix} \tag{9}$$

$$C = \begin{bmatrix} C(0) & 1 \\ C(1) & \\ C(2) & \\ \dots & \\ \dots & \\ C(m-1) & \\ \dots & \end{bmatrix} \tag{10}$$

An autoregressive filter is used to develop an error estimation model,  $\hat{E}$ The autoregressive filter can be defined as follows:

$$G = inv(R_{xx}^T \cdot R_{xx}) \cdot R_{xx}^T \cdot C \tag{11}$$

Where  $G$  is the AR filter,  $R_{xx}$  is the auto-correlation matrix of input matrix,  $C$  is the cross-correlation matrix between input and output.

A total of 52 cases between measured and ANN model is observed to get time series error. Figure 4 shows the basis of time series calculation to provide estimation of error signals for lift and drag forces. Previously, the neural nets are defined as feed forward multi layer systems which require an input vector, hidden and output layers. The input forms the instantaneous position in cross-flow direction, instantaneous position in in-line direction, instantaneous velocity in cross-flow direction and instantaneous velocity in in-line direction. Once error time series signals are observed for each case, eye inspection is applied by using auto-correlation analysis. This helps to categorize the error time series signals in order to be used for autoregressive filtering error estimation analysis. Autoregressive filter is applied to achieve error estimator for sample cases.  $\hat{E}(t)$  is estimated as a predicted error estimation from AR model. Then, we can express force signals as  $\hat{FAR} = \hat{FAN} + \hat{E} + \langle E \rangle$ . Where:  $\hat{FAR}$  is the ANN model with error predictor;  $\hat{FAN}$  is the ANN force model,  $\hat{E}$  is the error predictor from linear autoregressive filter and  $\langle E \rangle$  is the mean error between measured and ANN model. Then, error between measured and ANN model with error predictor can be calculated from  $F - \hat{FAR}$ .

**Results**

The purpose of this study is to develop data-driven models to model the dynamic forces acting on a vibrating circular cylinder in a free stream. While semi-empirical methods for modeling fluid forces in VIV rely on determination of force coefficients that are essentially cycle averaged representations of the force in phase with body motions, the present method allows for an approximation of discrete force values for a given set of kinematic conditions through the neural network representation. This has potential for improving fluid force modeling in conditions where limit cycles, or attractors of the dynamic system may be varying in time. It must be noted that the present study only looks at a very small subset of experimental force measurements from fixed motion conditions and these selected conditions have highly repeatable forces in time, which is favorable to the neural network method used. In conditions where multiple wake conditions may exist for a specific body

motion, more complex representation of the fluid force is likely necessary.

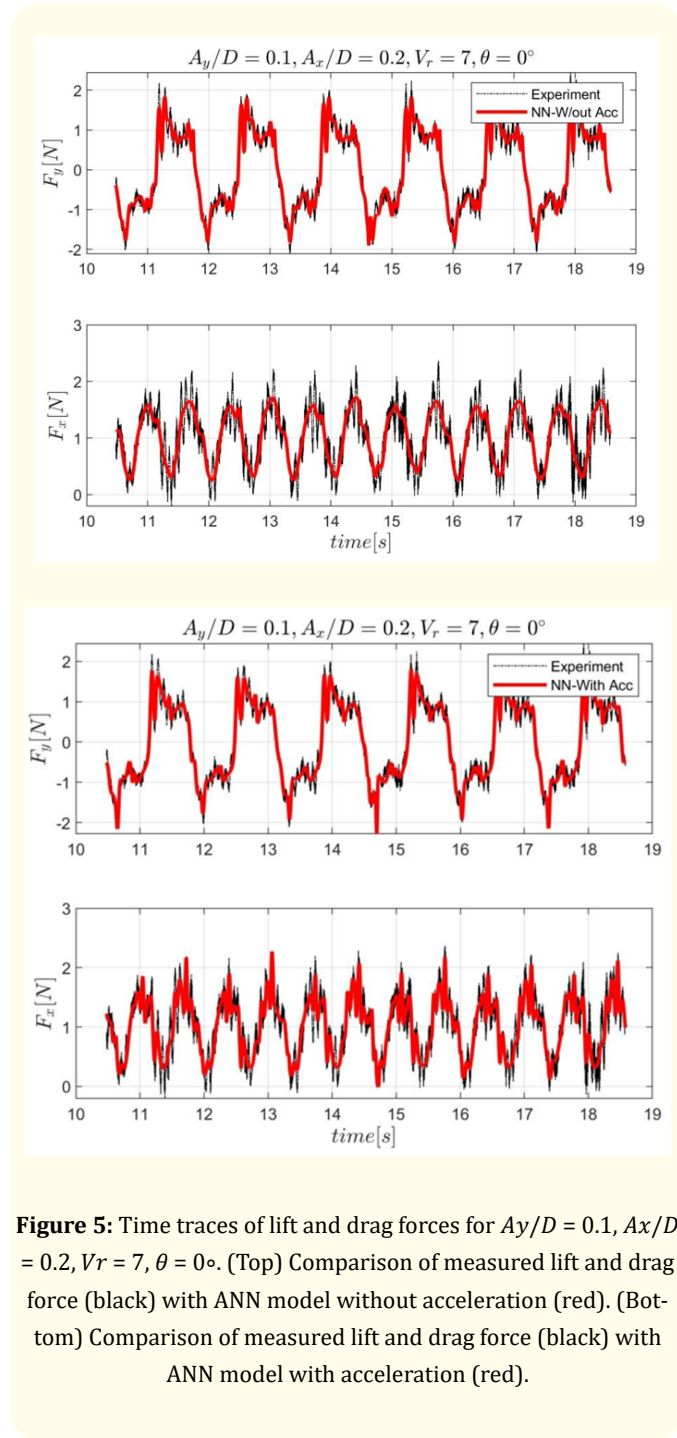


**Figure 5:** Time traces of lift and drag forces for  $A_y/D = 0.1, A_x/D = 0.2, V_r = 7, \theta = 0^\circ$ . (Top) Comparison of measured lift and drag force (black) with ANN model without acceleration (red). (Bottom) Comparison of measured lift and drag force (black) with ANN model with acceleration (red).

Experimental Input	Lift Force						
	Ax/D	Vr	$\theta$	Mean	Max	Mean	Max
Ay/D							
0.1	0.1	5	0	7.77	44.18	6.81	36.27
0.35	0.1	5	0	5.80	39.06	6.00	38.93
0.1	0.1	5	30	7.60	42.18	7.86	42.18
0.35	0.1	5	30	7.92	53.60	7.01	50.96
0.6	0.1	5	30	6.28	38.02	6.75	41.02
0.1	0.1	6	0	9.72	54.51	9.82	53.48
0.35	0.1	6	0	11.79	73.88	10.09	61.84
0.6	0.1	6	0	15.02	63.47	15.22	65.00
0.1	0.2	6	0	6.35	38.68	5.62	32.78
0.35	0.2	6	0	7.86	48.61	7.79	48.14
0.6	0.2	6	0	10.38	47.81	11.38	56.73
0.85	0.2	6	0	15.49	67.00	15.32	66.74
0.35	0.3	6	0	8.55	52.55	10.80	64.49
0.6	0.3	6	0	9.41	46.60	10.42	47.80
0.1	0.1	6	30	9.36	39.84	8.56	39.47
0.35	0.1	6	30	11.72	58.31	11.73	58.35
0.6	0.1	6	30	18.22	69.93	17.98	68.33
0.35	0.1	7	0	12.31	67.58	12.12	63.99
0.6	0.1	7	0	19.89	97.86	17.73	90.87
0.1	0.2	7	0	5.28	28.89	5.92	34.39
0.35	0.2	7	0	9.43	52.31	6.58	36.17
0.6	0.2	7	0	10.52	54.59	10.51	58.15
0.85	0.2	7	0	14.85	77.84	15.16	70.45
0.35	0.3	7	0	5.42	29.24	5.94	26.33
0.6	0.3	7	0	6.47	33.91	6.61	35.24
0.35	0.1	7	30	10.31	46.23	12.54	71.71
Column average				10.14	52.56	10.09	52.30
Column highest				19.89	97.86	17.98	90.87

**Table 1:** Mean and maximum errors (%) for all tested cases; Lift Force.

Table 1 and 2 show the mean and maximum percentage error between the measured and feed forward ANN estimation of lift and drag force time history using both the acceleration and without acceleration models:

$$E_{av} = 100 * \frac{mean(|F - \hat{F}|)}{max(|F|)}$$

$$E_{max} = 100 * \frac{max(|F - \hat{F}|)}{max(|F|)} \quad (12)$$

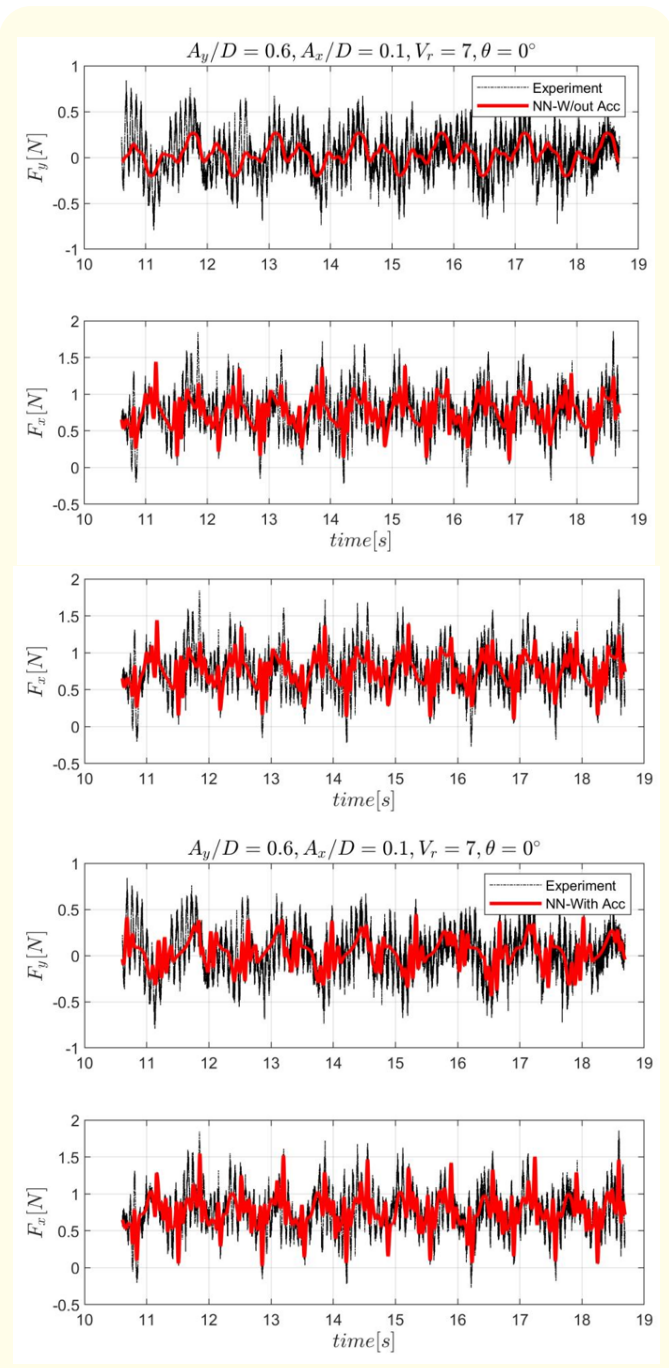


**Figure 6:** Time traces of lift and drag forces for  $A_y/D = 0.6$ ,  $A_x/D = 0.1$ ,  $V_r = 7$ ,  $\theta = 0^\circ$ . (Top) Comparison of measured lift and drag force (black) with ANN model without acceleration (red). (Bottom) Comparison of measured lift and drag force (black) with ANN model with acceleration (red).

Experimental Input	Drag Force							
	Without acc.		With acc.		Mean	Max	Mean	Max
$A_y/D$	$A_x/D$	$V_r$	$\theta$	0	Mean	Max	Mean	Max
0.1	0.1	5	0	5.98	33.84	7.16	37.71	
0.35	0.1	5	0	5.56	27.12	5.64	27.79	
0.1	0.1	5	30	6.34	32.20	7.12	33.09	
0.35	0.1	5	30	5.89	29.01	5.94	29.82	
0.6	0.1	5	30	5.35	34.99	5.27	29.70	
0.1	0.1	6	0	7.37	36.22	7.61	35.73	
0.35	0.1	6	0	8.80	36.00	8.67	43.90	
0.6	0.1	6	0	9.41	41.30	9.08	37.33	
0.1	0.2	6	0	4.93	27.49	4.95	31.12	
0.35	0.2	6	0	5.69	31.81	5.50	29.25	
0.6	0.2	6	0	7.38	31.98	6.53	30.76	
0.85	0.2	6	0	7.57	34.50	8.99	36.59	
0.35	0.3	6	0	7.39	28.31	5.42	25.75	
0.6	0.3	6	0	5.52	27.67	5.62	26.99	
0.1	0.1	6	30	7.86	40.33	8.55	43.49	
0.35	0.1	6	30	9.11	40.74	8.22	39.20	
0.6	0.1	6	30	8.40	40.31	8.55	43.11	
0.35	0.1	7	0	9.07	41.04	10.84	41.94	
0.6	0.1	7	0	9.10	41.95	8.59	41.95	
0.1	0.2	7	0	8.15	39.49	6.02	29.05	
0.35	0.2	7	0	8.11	38.90	5.73	34.55	
0.6	0.2	7	0	6.92	34.60	8.85	37.55	
0.85	0.2	7	0	7.35	35.70	7.27	35.56	
0.35	0.3	7	0	5.02	22.98	4.98	22.66	
0.6	0.3	7	0	5.67	30.43	6.80	40.82	
0.35	0.1	7	30	8.01	42.94	8.46	43.13	
Column average					7.15	34.69	7.17	34.94
Column highest					9.41	42.94	10.84	43.90

**Table 2:** Mean and maximum errors (%) for all tested cases; Drag Force.

Where:  $E_{av}$  is the percentage mean error which is calculated from between measured,  $F$  and estimated  $\hat{F}$  response for all cases.  $E_{max}$  is the percentage maximum error which is calculated from between measured,  $F$  and estimated  $\hat{F}$  response for all cases as well. The tables give the computed error for the 26 different kinematic motions of the cylinder, showing the error for the two separate models for lift and drag. The tables show the total mean and maximum errors with and without acceleration cases for lift and drag forces. Comparing the measured error between the model which includes acceleration components and the model that is trained purely on position and velocity, the model including acceleration appears to

have less overall error, which is not surprising, as the added mass force of the fluid is dependent on the body acceleration, hence will be poorly estimated by position only, especially if significant non-linear effects are present.

Figure 5 shows the time history of cross-flow and in-line measured forces based on experimental conditions of  $Ay/D = 0.1$ ,  $Ax = 0.2$ ,  $Vr = 7$ ,  $\theta = 0^\circ$  compared with the resulting fluid force estimates obtained through the neural networks models. As seen from the time histories, 6 cycles of motion were observed for this particular case (dependent on the tank length and reduced velocity) in the cross-flow direction. The measured (black) and predicted (red) forces are compared for the both the model which includes the acceleration and the model without the acceleration. Immediately apparent from the figures is that the model without acceleration tends to smooth out much of the higher frequency components of the signal. This is not necessarily a good thing, since in combined in-line and cross-flow motion, the relative motion of the body in the in-line direction with respect to vortices shed in the wake can enhance the presence of higher frequency components of force acting on the cylinder [8]. In the lift direction, these forces will show up as odd harmonics and are a result of the non-linear interaction of the body motion and vortex motion. In the drag direction, these forces manifest as higher even harmonics. The ANN model with acceleration appears to do significantly better with capturing higher harmonic components of force, which are important when modeling fatigue effects of VIV. This particular case represents a relatively small cross-flow motion of the body and the resulting force model has relatively low error as seen in the previous tables.

To give another example with larger cross-flow amplitude, figure 6 shows the time history of cross-flow and in-line measured forces based on experimental conditions of  $Ay/D = 0.6$ ,  $Ax = 0.1$ ,  $Vr = 7$ ,  $\theta = 0^\circ$  compared with the resulting fluid force estimates obtained through the neural networks models. In this case, again the fluid force model with acceleration captures more of the higher frequency components of the signal. In this case, we observe relatively large mean and maximum errors between measured and ANNs estimation for both lift and drag force which can be seen from table 1 and 2. In this case, some of the error is likely due to the mechanical vibration of the cantilevered cylinder below the force sensor at its natural frequency.

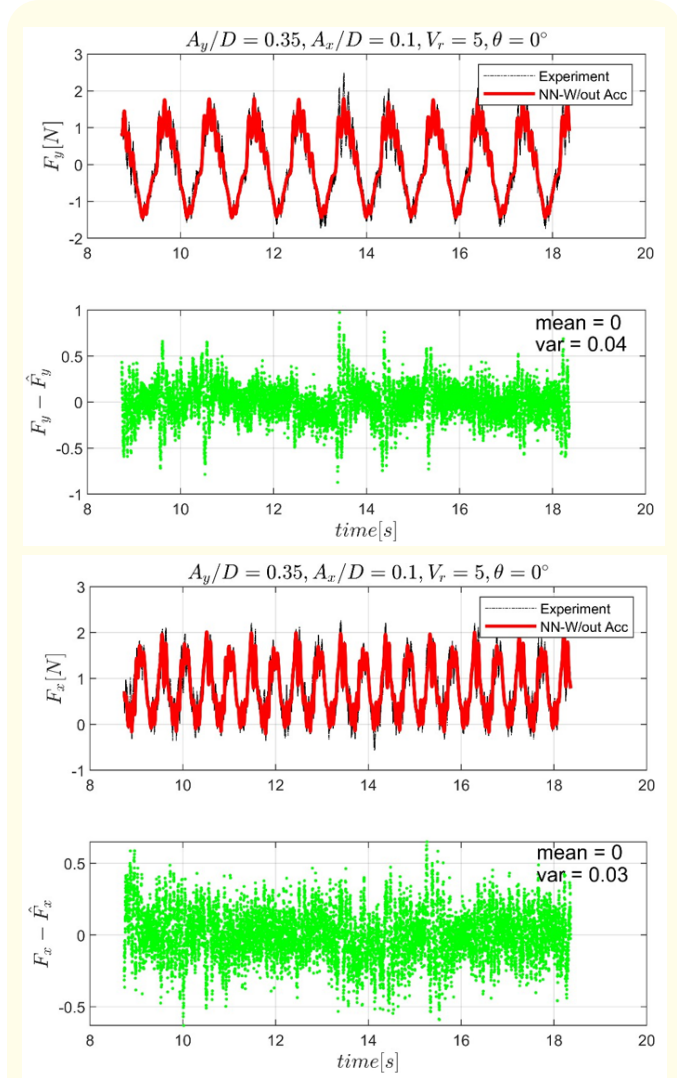
After building ANN force model, we develop error estimation model from measured forces acting on an oscillating cylinder in

free stream and neural network model. We use only without acceleration case in order to build error estimation model since the average errors between ANN force model and force measurements are very close for with and without acceleration cases. Error estimation model allows to correct ANN model based on measured forces. The error estimation model is applied for the same small subset of the experimental force database. However, once error estimators are achieved, this can help to generalize later to develop dynamical systems. Currently, again error estimation model is applying highly repeatable forces which is suitable to the ANN and error estimation model. They may exist multiple wake conditions for specific conditions where more complex representation of the fluid force could be necessary.

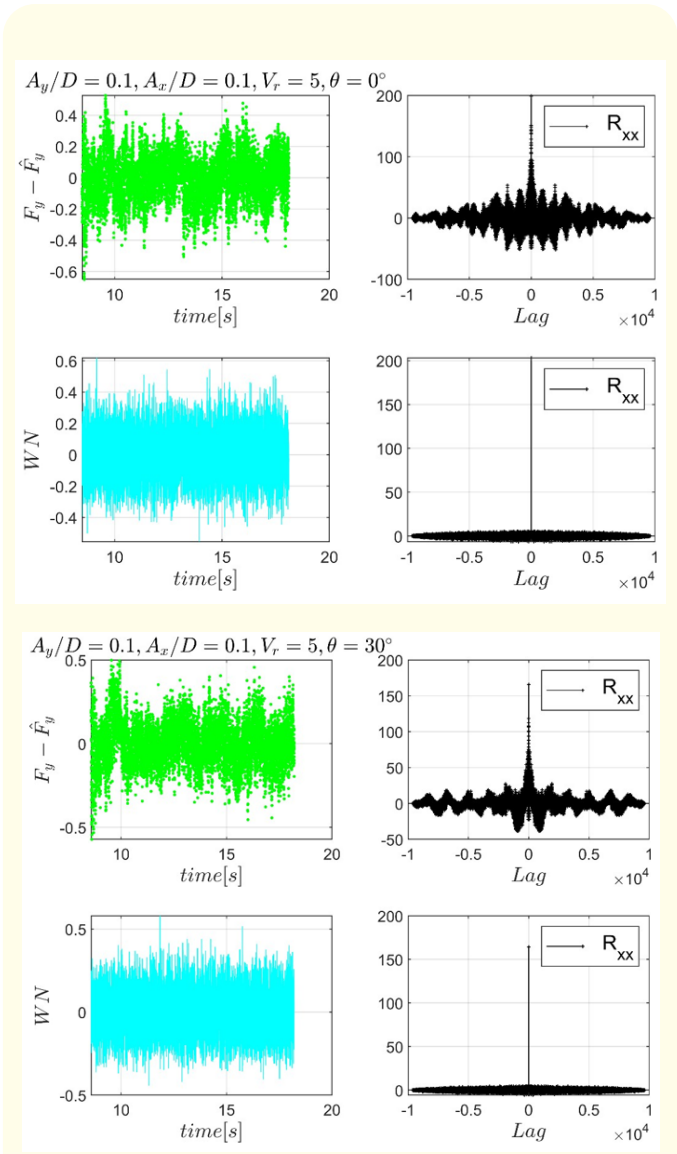
Figure 7 shows the time trace of error between ANN model and measured fluid forces for lift and drag forces. Errors,  $E$  is the are the time series errors which are calculated from between measured,  $F$  and estimated ANN model  $\hat{ANN}$  response for all cases. This plot shows two specific computed errors among these sub-database. Actually, errors are calculated for 26 different kinematic motions of the circular cylinder. These errors are calculated for two separate models; lift and drag forces. The measured error between the model do not include acceleration components and the model that is trained purely on position and velocity inputs. As we can see from the figures, the errors have still structural response which can contribute to force model. Along with these information, auto-correlation analysis are applied for all subdatabase to observe structural category for these errors in order to be used to estimate errors later.

Figure 8 and 9 shows the time history of errors for lift direction and auto-correlation analysis of these error signals for cross-flow direction for some specific kinematics of the circular cylinder. Also random white noises are generated with same mean and standard deviation of each error signals which shows different autocorrelation structure from error signals from cross-flow direction. Autocorrelation of errors are calculated for lift and drag direction observe category in error analysis in order to build error model. However, the lift direction errors are used to observe category for error signals since cross-flow direction is the leading direction for two-degree-of-freedom cases. As we observe from the sub-data set in free vibration regime, 4 different category are observed from auto-correlation analysis.  $Ay/D = 0.1$ ,  $Ax/D = 0.1$ ,  $Vr = 5$ ,  $\theta = 0^\circ$  and  $Ay/D = 0.1$ ,  $Ax/D = 0.1$ ,  $Vr = 5$ ,  $\theta = 30^\circ$  and  $Ay/D = 0.6$ ,  $Ax/D = 0.1$ ,  $Vr = 5$ ,  $\theta = 30^\circ$  and  $Ay/D = 0.35$ ,  $Ax/D = 0.1$ ,  $Vr = 6$ ,  $\theta = 0^\circ$  represents

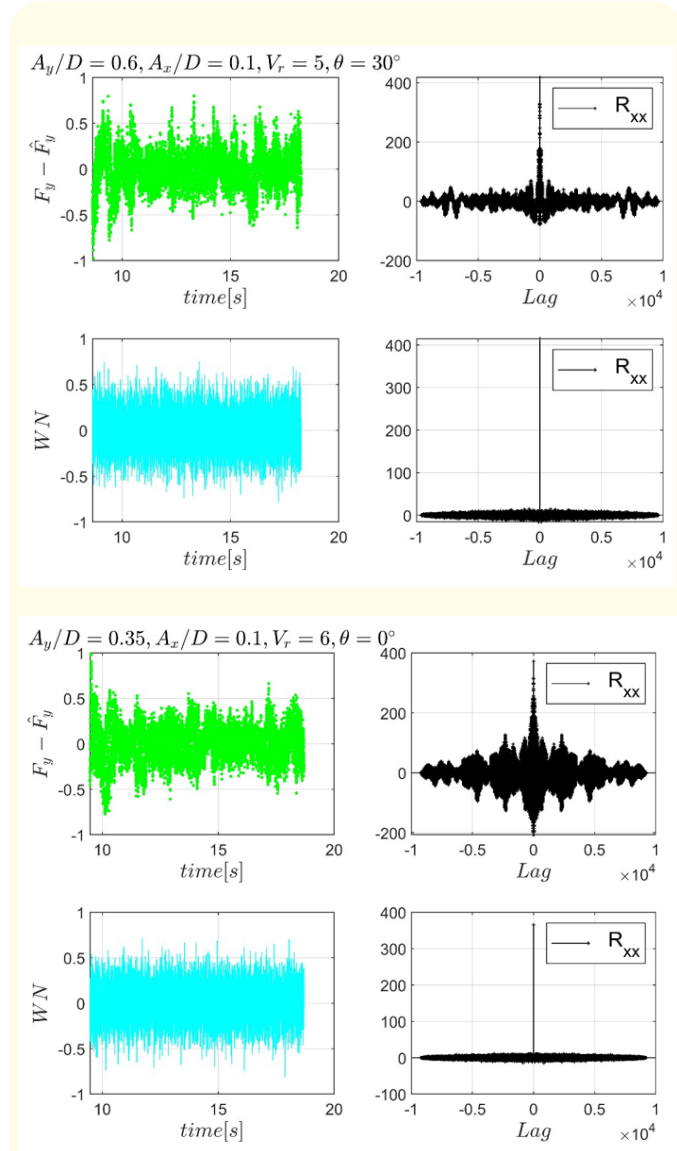
a chosen case for different categories in sub- database. Knowing these categories are important because these information could improve error estimation model.



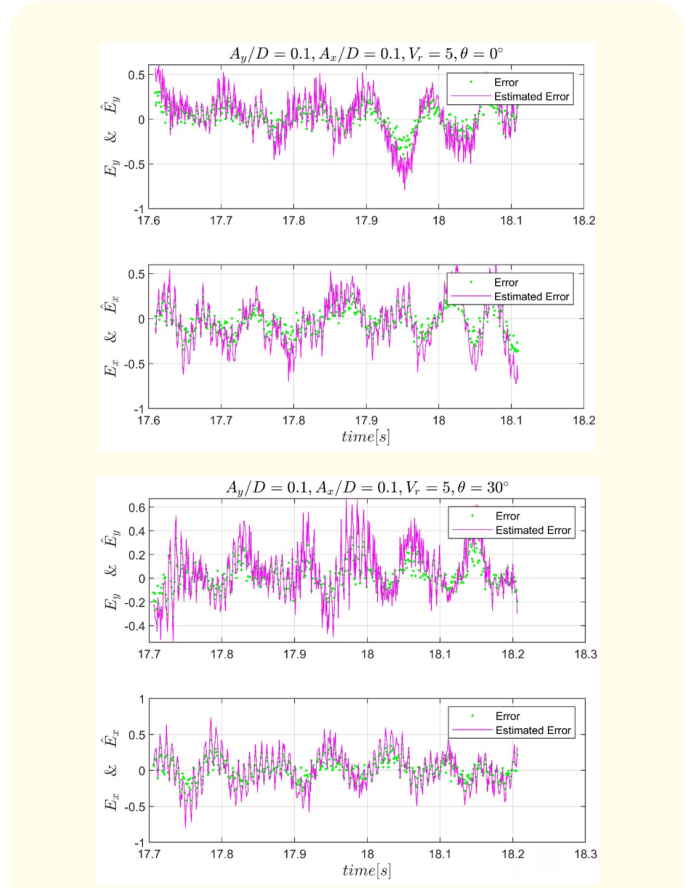
**Figure 7:** (Top) Comparison of measured (black) and ANN model (red) for time traces of lift force and the corresponding time trace of error between measured and ANN model (green) on top plot; (bottom) Comparison of measured (black) and ANN model (red) for time traces of drag force and the corresponding time trace of error between measured and ANN model (green) on bottom plot for a specific run:  $A_y/D = 0.35, A_x/D = 0.1, V_r = 5, \theta = 0^\circ$ .



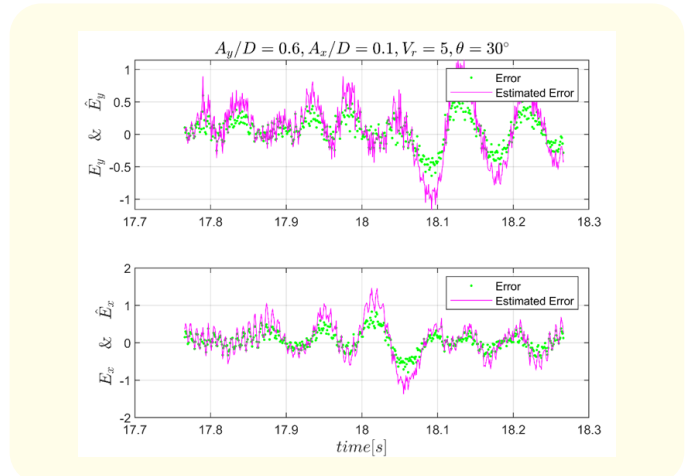
**Figure 8:** The time trace of error for lift force and auto-correlation of the lift force error which corresponding and white noise corresponding to lift force and the auto-correlation of this white noise on top plot and the time trace of error for drag force and auto-correlation of the drag force error which corresponding and white noise corresponding to drag force and the auto-correlation of this white noise on bottom plot:  $A_y/D = 0.1, A_x/D = 0.1, V_r = 5, \theta = 0^\circ$  and  $A_y/D = 0.1, A_x/D = 0.1, V_r = 5, \theta = 30^\circ$ : Category 1 and Category 2.

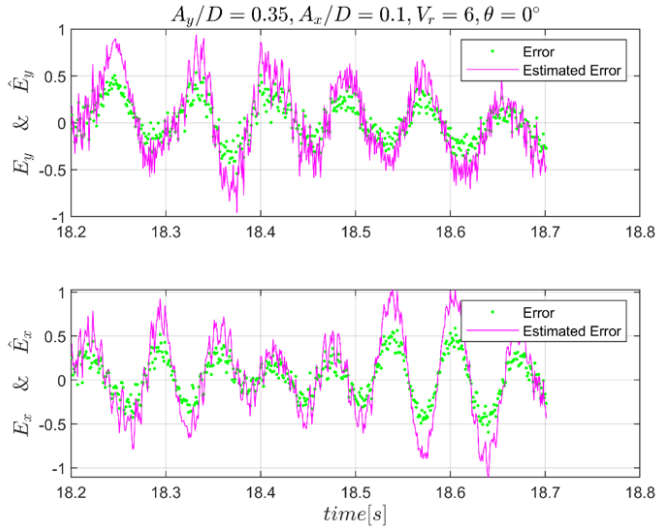


**Figure 9:** The time trace of error for lift force and auto-correlation of the lift force error which corresponding and white noise corresponding to lift force and the auto-correlation of this white noise on top plot and the time trace of error for drag force and auto-correlation of the drag force error which corresponding and white noise corresponding to drag force and the auto-correlation of this white noise on bottom plot:  $A_y/D = 0.6, A_x/D = 0.1, V_r = 5, \theta = 30^\circ$  and  $A_y/D = 0.35, A_x/D = 0.1, V_r = 6, \theta = 0^\circ$ : Category 3 and Category 4.

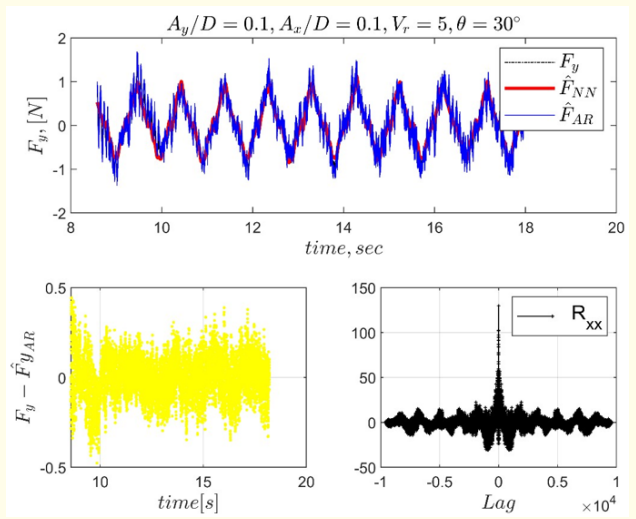


**Figure 10:** The last portion of time series error estimation for cross-flow and in-line direction:  $A_y/D = 0.1, A_x/D = 0.1, V_r = 5, \theta = 0^\circ$  and  $A_y/D = 0.1, A_x/D = 0.1, V_r = 5, \theta = 30^\circ$ : Category 1 and Category 2.

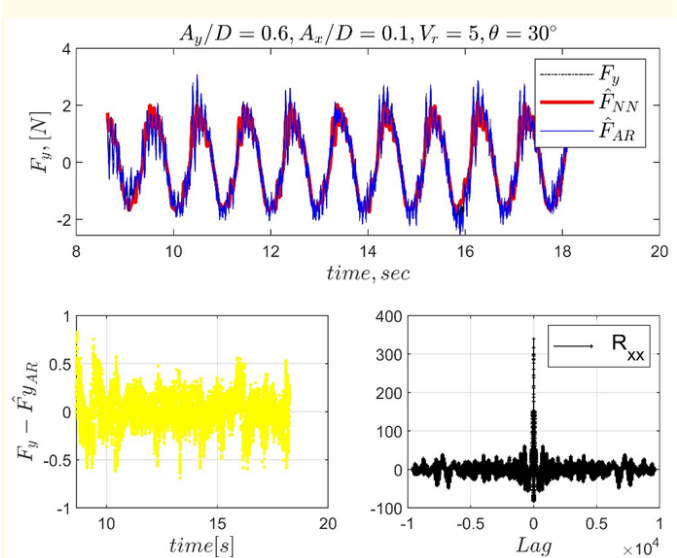
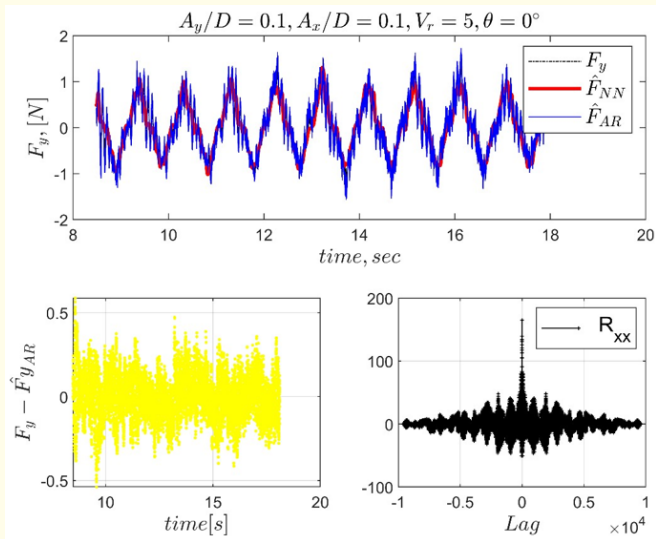




**Figure 11:** The last portion of time series error estimation for cross-flow and in-line direction:  $A_y/D = 0.6, A_x/D = 0.1, V_r = 5, \theta = 30^\circ$  and  $A_y/D = 0.35, A_x/D = 0.1, V_r = 6, \theta = 0^\circ$ : Category 3 and Category 4.



**Figure 12:** Comparison of measured (black), ANN model (red) and ANN model with error predictor (blue) for time traces of lift force and the time trace of error between measured and new estimated force with error predictor:  $A_y/D = 0.1, A_x/D = 0.1, V_r = 5, \theta = 0^\circ$  and  $A_y/D = 0.1, A_x/D = 0.1, V_r = 5, \theta = 30^\circ$



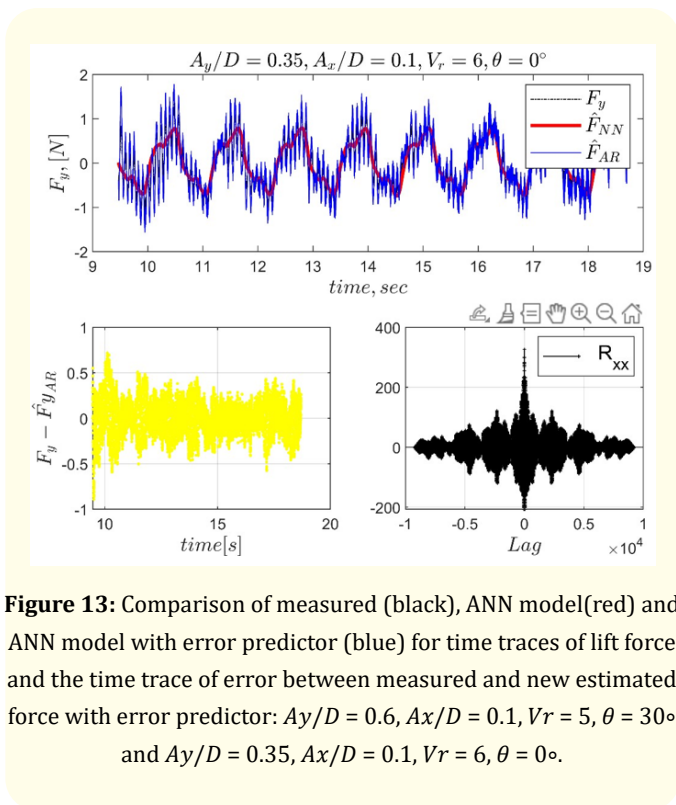


**Figure 13:** Comparison of measured (black), ANN model (red) and ANN model with error predictor (blue) for time traces of lift force and the time trace of error between measured and new estimated force with error predictor:  $A_y/D = 0.6, A_x/D = 0.1, V_r = 5, \theta = 30^\circ$  and  $A_y/D = 0.35, A_x/D = 0.1, V_r = 6, \theta = 0^\circ$ .

Figure 10 and 11 show the results of error estimations for each category which is observed in sub- database. The linear autoregressive filter is used to develop the error estimation model. Green dotline shows the last time portion of the error between measured forces and ANN force model for both cross- flow and in-line direction. The magenta line shows the estimated error by using linear predictor filter for both cross-flow and in-line direction. Linear autoregressive filter is applied for one sample from each category. Therefore, the error estimation represents for each category which is observed by eye before using auto-correlation analysis. The main purpose of this error estimation analysis is to improve ANN force model which is going to be applied all database later. Error estimation model improves the force model by superimposing the ANN force estimation.

Figure 12 and 13 show the comparison result between time trace of measured force, ANN force model and ANN model with error predictor for lift force. The results are shown for chosen cases for each error category which is described before. One can observe the error signals between measured force and ANN model with corrected error predictor. Also, we observe a better approximation by using error predictor in comparison with ANN force model. Auto-

correlation analysis can be seen from the figures as well.

$E_{av}$  is the percentage mean error where it is calculated from measured,  $F$  and for both estimated ANN force model,  $\hat{F}_{NN}$  and both estimated ANN force model with error predictor,  $\hat{F}_{AR}$  for all sample cases from each category.  $E_{max}$  is the percentage maximum error where it is calculated from between measured,  $F$  and estimated ANN force model  $\hat{F}_{NN}$  and ANN force model with error predictor,  $\hat{F}_{AR}$  response for all sample cases from each category as well. The table provides the computed error for 4 different kinematic motions of the cylinder which shows the total mean and maximum errors for the lift force. The table shows the total mean and maximum errors for ANN model force model and ANN model with error predictor: Comparing the calculated error between the model such that the ANN model with error prediction shows better estimation than ANN force model. This shows that error estimation model helps to improve ANN model.

Experi- mental Input	Lift Force						
	ANN model			ANN model			
	w\out acc.			w\Err. Predictor			
$A_y/D$	$A_x/D$	$V_r$	$\theta$	mean	max	mean	max
0.1	0.1	5	0	7.77	44.18	5.27	26.78
0.1	0.1	5	30	7.60	42.18	5.63	28.38
0.6	0.1	5	30	6.28	38.02	4.69	28.13
0.35	0.1	6	0	11.79	73.88	8.36	33.56
Column average				8.36	49.56	5.98	29.22
Column highest				11.79	73.88	8.36	33.56

**Table 3:** Mean and maximum errors (%) for all tested cases; Lift force.

**Discussion**

One can see that ANN force model and error prediction model is developed from very small subset of experimental data which includes force measurements from fixed motion parameters. Also, it must be note that this selected sub-database includes highly repeatable forces with time. Thus, it helps neural networks applications for developing models. On the other hand, there are some observed cases where multiple wake conditions may exist for a specific body motion which means more complex representation of the fluid force may be necessary.

As seen from the comparisons, the feed forward neural nets achieve satisfactory accuracy for the chosen subset of experiments.

ANN force model results in matching the measured data series for both models with and without acceleration. VIV systems are typically self-limiting oscillations and autonomous models can achieve self-limiting oscillations. This limitation can be verified by evaluation of the Lyapunov exponent analysis [37]. In future work, we intend to improve and extend this model to feedback control synthesis toward energy harvesting applications.

One can observe a better approximation by using an error predictor in comparison with the ANN force model. This preliminary result shows better force estimation with error predictor where an autoregressive filter is used to develop the error estimation model. This method will be applied to correct ANN force model for the whole database in order to develop further dynamic models.

The main advantage of developing an ANN model with error prediction for a sub-region of the force database is that it creates a general model for VIV forces, which typically in the literature involve a second-order ordinary differential equation driven by external hydrodynamic forcing. Instead, the general model consists of an autonomous dynamical system of the same order. Autonomous systems, by definition, do not require an external forcing to drive their dynamics. This allows for deeper investigations and improved insight of the system dynamics since all features are incorporated in the model structure rather than being split between the forcing and the model structure. Further advances can thus be enabled by employing the insightful and powerful mathematical theory for dynamical systems encompassing tools and techniques like phase portraits, Poincare maps, recurrence plots etc.

## Conclusion

This study shows an ANN force model and error estimation model for the forces acting on a circular cylinder undergoing controlled combined in-line and cross-flow motion in a free stream. The ANN force model is developed using an artificial neural network approach. Neural networks are trained by utilizing time dependent force measurements obtained through experiments to train weights and biases necessary to model the time dependent forces as a function of instantaneous kinematic conditions. The feed forward neural networks provide a closed-form explicit mathematical relationship for modeling the forces. The error estimation model is developed using linear autoregressive filter. Linear predictor filter is applied for sub-database from error between measured and ANN force model. The result of error predictor are shown for each ob-

served error category which is investigated by using autocorrelation analysis in sub-database. This error estimation model is used to help improving ANN force model by superimposing into ANN time series force estimation. This large comprehensive dataset will be used for more deep learning analysis. Force prediction method will be developed from an oscillating circular cylinder from forced experiments by using neural networks applications. These techniques can be used for a non-linear force control model which might be developed to predict fluid-structure interactions. The developed model will be applied for future control models energy harvesting applications by using whole database.

## Bibliography

1. Sarpkaya T. "Vortex-Induced Oscillations: A Selective Review". *Journal of Applied Mechanics* 46.2 (1979): 241-258.
2. Bearman PW. "Vortex Shedding from Oscillating Bluff Bodies". *Annual Review of Fluid Mechanics* 16.1 (1984): 195-222.
3. Parkinson G. "Phenomena and modelling of flow-induced vibrations of bluff bodies". *Progress in Aerospace Sciences* 26.2 (1989): 169-224.
4. Sarpkaya T. "A critical review of the intrinsic nature of vortex-induced vibrations". *Journal of Fluids and Structures* 19.4 (2004): 389-447.
5. Williamson CHK and Govardhan R. "Vortex-Induced Vibrations". *Annual Review of Fluid Mechanics* 36.1 (2004): 413-455.
6. Bearman PW. "Circular cylinder wakes and vortex-induced vibrations". *Journal of Fluids and Structures* 27.5-6 (2011): 648-658.
7. Lee JH., et al. "Virtual damper-spring system for VIV experiments and hydrokinetic energy conversion". *Ocean Engineering* 38.5-6 (2011): 732-747.
8. Dahl JM., et al. "Resonant Vibrations of Bluff Bodies Cause Multivortex Shedding and High Frequency Forces". *Physical Review Letters* 99.14 (2007): 144503.
9. Dahl JM., et al. "Dual resonance in vortex-induced vibrations at subcritical and supercritical Reynolds numbers". *Journal of Fluid Mechanics* 643 (2010): 395-424.
10. Jauvtis N and Williamson CHK. "The effect of two degrees of freedom on vortex-induced vibration at low mass and damping". *Journal of Fluid Mechanics* 509.509 (2004): 23-62.

11. Staubli T. "Calculation of the Vibration of an Elastically Mounted Cylinder Using Experimental Data From Forced Oscillation". *Journal of Fluids Engineering* 105.2 (1983): 225-229.
12. Gopalkrishnan R. "Vortex-Induced Forces on Oscillating Bluff Cylinders" (1983).
13. Morse TL and Williamson CHK. "Employing controlled vibrations to predict fluid forces on a cylinder undergoing vortex-induced vibration". *Journal of Fluids and Structures* 22.6-7 (2006): 877-884.
14. Morse TL and Williamson CHK. "Prediction of vortex-induced vibration response by employing controlled motion". *Journal of Fluid Mechanics* 634 (2009): 5-39.
15. Chaplin JR., et al. "Blind predictions of laboratory measurements of vortex-induced vibrations of a tension riser". *Journal of Fluids and Structures* 21 (2005): 25-40.
16. Bernitsas MM., et al. "Eigen-Solution for Flow Induced Oscillations (VIV and Galloping) Revealed at the Fluid-Structure Interface". *CFD and FSI 2* (2019).
17. Liu C., et al. "Time-varying hydrodynamics of a flexible riser under multi-frequency vortex-induced vibrations". *Journal of Fluids and Structures* 80 (2018): 217-244.
18. Liu C., et al. "Hydrodynamics of a flexible cylinder under modulated vortex-induced vibrations". *Journal of Fluids and Structures* 94 (2020): 102913.
19. Dahl JJM. "Vortex-induced vibration of a circular cylinder with combined in-line and cross-flow motion" (2008).
20. Zheng H., et al. "Coupled Inline-Cross Flow VIV Hydrodynamic Coefficients Database". *CFD and VIV 2* (2014).
21. Aktosun E and Dahl JM. "Experimental Force Database From Controlled In-Line and Cross Flow Cylinder Motion". The 28th International Ocean and Polar Engineering Conference (2018).
22. Dahl J and Aktosun E. "Force and wake observations for a circular cylinder undergoing forced 2-DOF motion in a free stream". *APS* (2019): C48--004.
23. Dahl JM., et al. "Two-degree-of-freedom vortex-induced vibrations using a force assisted apparatus". *Journal of Fluids and Structures* 22.6-7 (2006): 807-818.
24. Tsoukalas LH and Uhrig RE. "Fuzzy and neural approaches in engineering" (1997).
25. Fausett L. "Fundamentals of Neural Networks Prentice Hall". Englewood Cliffs, NJ (1994): 7632.
26. Ogunfunmi T. "Adaptive nonlinear system identification: The Volterra and Wiener model approaches" (2007).
27. Zaknich A. "Principles of adaptive filters and self-learning systems" (2005).
28. Xiros NI. "Digital Signal Processing". *Springer Handbook of Ocean Engineering* (2016): 197-226.
29. Xiros NI and An P-CE. "Control Theory and Applications". *Springer Handbook of Ocean Engineering* (2016): 227-276.
30. Klamo JT, et al. "On the maximum amplitude for a freely vibrating cylinder in cross-flow". *Journal of Fluids and Structures* 21.4 (2005): 429-434.
31. Hsu HP. "Theory and problems of probability, random variables, and random processes". 83 (1996).
32. Castanié F. "Digital Spectral Analysis" (2011).
33. Orfanidis SJ. "Applied Optimum Signal Processing" (2018).
34. Bracewell RN and Bracewell RN. "The Fourier transform and its applications". 31999 (1986).
35. Wolovich WA. "Linear Multivariable Systems" (1974).
36. Aktosun E., et al. "A neural network time dependent hydrodynamic force model for forced two-degree-of-freedom sinusoidal motion of a circular cylinder in a free stream". *ASME 2021 40th International Conference on Ocean, Offshore and Arctic Engineering* (2021).
37. Xiros NI., et al. "Dynamic Modeling of Flow Induced Vibration Power-Plants". *International Conference on Offshore Mechanics and Arctic Engineering* 51319 (2018): V010T09A009.

**Volume 3 Issue 8 August 2021**

© All rights are reserved by Nikolaos I Xiros., et al.